REPORT DOCUMENTATION PAGE

Form Approved OMB No. 0704-0188

1. AGENCY USE ONLY (Leave blank)	2. REPORT DATE	3. REPORT TYPE AND DATES COVERED
		Final Report

4. TITLE AND SUBTITLE

Plasma Treatment Of Surfaces And Plasma Enhanced Deposition

5. FUNDING NUMBERS

F6170896W0162

6. AUTHOR(S)

Prof. Daniel Schram

7. PERFORMING ORGANIZATION NAME(S) AND ADDRESS(ES)

Eindhoven University of Technology
P.O. Box 513
Eidhoven 5600 MB
Netherlands

8. PERFORMING ORGANIZATION REPORT NUMBER

N/A

9. SPONSORING/MONITORING AGENCY NAME(S) AND ADDRESS(ES)

EOARD
PSC 802 BOX 14
FPO 09499-0200

10. SPONSORING/MONITORING AGENCY REPORT NUMBER

SPC 96-4016

11. SUPPLEMENTARY NOTES

12a. DISTRIBUTION/AVAILABILITY STATEMENT

Approved for public release; distribution is unlimited.

12b. DISTRIBUTION CODE

A

13. ABSTRACT (Maximum 200 words)

This report results from a contract tasking Eindhoven University of Technology as follows: The contractor will investigate the plasma treatment of surfaces and plasma enhanced deposition using EUT's cascade arc source as the basis for this effort.

14. SUBJECT TERMS

Plasma Physics

15. NUMBER OF PAGES

19

16. PRICE CODE

N/A

17. SECURITY CLASSIFICATION OF REPORT	18. SECURITY CLASSIFICATION OF THIS PAGE	19. SECURITY CLASSIFICATION OF ABSTRACT	20. LIMITATION OF ABSTRACT
UNCLASSIFIED	UNCLASSIFIED	UNCLASSIFIED	UL

Eindhoven University of Technology

Final Report

European Office of Aerospace
Research and Development
Contract no.: SPC-96-4016

VDF/NT 97-30

This report is part of an ongoing cooperation between the Eindhoven University of Technology and the Wright Laboratories at Dayton, Ohio. This work has been sponsored by the EOARD under contract no. SPC-96-4016.

The results described in this report were presented at the International Symposium on Plasma Chemistry (ISPC-13, Beijing, China, 18-22 August 1997).

Department of Physics
Eindhoven University of Technology
P.O.Box 513
5600 MB Eindhoven
The Netherlands

Contents

Ion densities in a high intensity, low flow nitrogen plasma

G.J.H. Brussaard, M.C.M. van de Sanden, and D.C. Schram
Department of Physics, Eindhoven University of Technology, P.O.Box 513,
5600 MB Eindhoven, The Netherlands

ABSTRACT: The plasma density in an expanding thermal plasma was determined using planar Langmuir probe measurements. The arc plasma was operated at low flow (500 standard cm^3 per minute). To improve reliability at these low flows, an arc was constructed with a variable channel diameter. This seems to lead to a slightly higher ion density at the exit of the arc when running an argon plasma. In the case that nitrogen is injected in the arc the plasma density is lowered considerably due to charge exchange and dissociative recombination in the expansion. Because of the low electron density (10^{17} m^{-3}) at a partial nitrogen flow larger than 10%, the dissociative recombination becomes slow. The dominant ion in this case is the molecular ion N_2^+. The main loss process of N_2^+ ions in this case is diffusion away from the plasma axis. The effective decay length found in the nitrogen plasma is 9 cm. This is comparable to Ar^+ in argon at the same pressure.

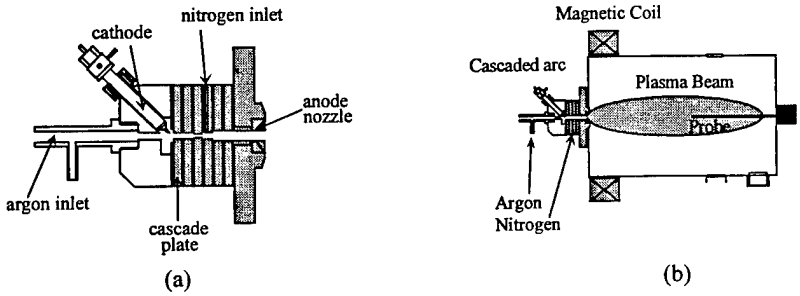

Figure 1: Cascaded arc (a) and expanding plasma setup (b).

I. INTRODUCTION

High density plasmas are commonly used in a variety of industrial applications1. Some of these sources are used as downstream sources where the plasma production is separated from the treatment region. One such source is the expanding thermal arc [Figure (1)] under investigation at the Eindhoven University of Technology [2, 3]. The arc is usually operated at flows of 1000 to 10000 standard cm^3 per minute (sccm). Because in many industrial applications pump capacity is limited the question arose to modify the plasma source to work at lower flows. To be able to use the

plasma at flow rates in the range of 100-500 sccm, the bore of the copper plates was varied. It was found that operation was most reliable if six plates were used with bores varying between 4 and 1 mm. The fourth plate, with a bore of 2 mm contains a seeding channel, through which nitrogen can be flowed into the arc. An overview of the relevant parameters during the experiments is given in Table I.

Table I: Overview of experimental conditions

Ar flow	500-100 sccm
N_2 flow	0-400 sccm
Arc current	36 A
Downstream ($z > 10$ cm):	
Chamber pressure	7 Pa
Electron density	10^{17} - 10^{19} m^{-3}
Electron temperature	0.1 - 0.3 eV
Gas temperature	300 - 500 K

This report investigates the working of the arc by comparing the ion density in the low flow argon plasma to the expanding plasma during normal (higher flow) operation [2]. Then the ion density and distribution is investigated when nitrogen is added. A model for the gas phase reactions involving ions in the nitrogen plasma is compared to the experimental results.

II. EXPERIMENTS

A planar Langmuir probe with a radius of 2 mm is placed on the expansion axis of the plasma with the normal to the probe surface parallel to the expansion. The probe can be controlled by a movable arm to measure at different positions in the plasma. Measurements are taken as a function of distance from the nozzle (10 - 21 cm) and as a function of ratio argon to nitrogen flow into the arc (0% - 80%).

III. ARGON PLASMA

A pure argon plasma was created with a total flow of 500 sccm. Because extensive research has been carried out on the expanding argon jet [2, 4, 5] this plasma can be used to investigate the differences in the workings of the arc under the conditions of low flow. The electron density was measured by the Langmuir probe, as a function of distance from the nozzle. The results are shown in Figure 2. If the densities are extrapolated to $z = 0$, a density of n_{e0} of 9.4×10^{18} m^{-3} is found. This can be compared to results in the high flow regime (flow > 3500 sccm) by Van de Sanden et al. [2]. who found that the ion density scales approximately linearly with arc current and background pressure. A comparison between their results and the value found here is given in Figure 3. The initial density in the plasma under investigation in this report is a factor of 2 higher. This may be attributed to a relatively higher pressure inside the arc caused by the smaller bore of the central plates used when operating at lower flow.

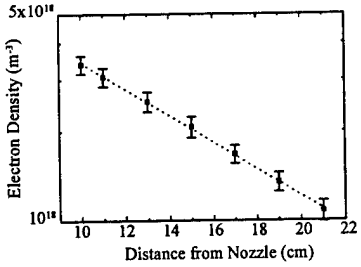

Fgure 2: Electron density as a function of distance from the nozzle in argon. The dashed line shows an exponential decrease with an effective decay length of 10 cm.

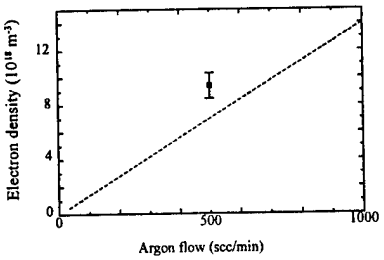

Figure 3: Extrapolated initial densities in argon as a function of gas flow. The dashed line shows the empirical relation found by van de Sanden et al. [2]. The square (■) is the extrapolation of Fig. 4.

IV. NITROGEN PLASMA

The results found in argon can now be used as a basis for understanding the results in the nitrogen/argon mixtures. Inside the arc the temperatures are high ($T_h \approx T_e \approx 1$ eV) and so is the electron density ($n_e \approx 10^{22}$ m^{-3}). Therefore, the relative abundance of the ions can be calculated using pLTE considerations. The ions will be atomic ions only and their relative density is given by

$$\frac{n_{N^+}}{n_{Ar^+}} = \frac{g(N^+)}{g(N)} \frac{g(Ar)}{g(Ar^+)} \frac{N_{flow}}{Ar_{flow}} e^{\left(\frac{E_{Ar^+} - E_{N^+}}{T_e}\right)} \quad (1)$$

with n_{N^+}, n_{Ar^+} the density of N^+ and Ar^+, g(..) the statistical weights of the different particles, and $E_{..}$ the ionization energy for each atom. For the purpose of modeling and understanding the reactions taking place in the expansion, it is assumed that the relative density given by Eq.(1) still exists just after the shock in the expansion. The influence of varying the relative flow of the gases into the arc on the electron density on the expansion axis, at a distance of 15 cm from the nozzle, is shown in Figure 4. These results can be explained using charge exchange and dissociative recombination as the main loss proces of ions in the gas phase. The dissociated and ionized gas coming from the arc expands into a background of neutral argon and molecular nitrogen formed on the vessel walls. The following reactions will then determine the densities of the different species:

- Charge exchange

$$Ar^+ + N_2 \rightarrow Ar + N_2^+, \quad \text{rate } k_1 \quad (2)$$

$$N^+ + N_2 \rightarrow N + N_2^+, \quad \text{rate } k_2 \quad (3)$$

- Recombination:

$$N_2^+ + e \rightarrow N^* + N, \quad \text{rate } k_3 \tag{4}$$

At $T_e \approx 0.2$ eV, the charge exchange rates k_1 and k_2 are estimated to be 7×10^{-17} m^3s^{-1} [6] and 1×10^{-16} m^3s^{-1} [7] respectively. The rate of the dissociative recombination, k_3, is estimated at 10^{-13} m^3/s [8]. With a drift velocity of 600 m/s [2] and the rates given above, diffusion away from the expansion axis is negligible compared to charge exchange and recombination for a relative nitrogen flow above approximately 1% and electron densities larger than 10^{17} m^{-3}. This is also shown by the dashed line in Fig.(3). Reactions (2) through (4) can now be rewritten as a set of rate equations:

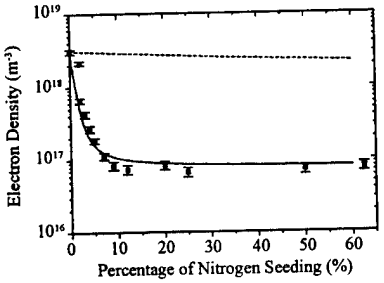

Figure 4: Electron density at 15 cm from the nozzle as a function of relative nitrogen flow. The dashed line shows the influence of diffusion, the solid line shows the recombination.

$$\frac{\partial n_{Ar^+}}{\partial z} = -k_1 n_{Ar^+} n_{N_2} \frac{1}{v_d} \tag{5}$$

$$\frac{\partial n_{N^+}}{\partial z} = -k_2 n_{N^+} n_{N_2} \frac{1}{v_d} \tag{6}$$

$$\frac{\partial n_{N_2^+}}{\partial z} = k_1 n_{Ar^+} n_{N_2} \frac{1}{v_d} + k_2 n_{N^+} n_{N_2} \frac{1}{v_d} - k_3 n_{N_2^+} n_e \frac{1}{v_d} \tag{7}$$

where $n_e = n_{Ar^+} + n_{N^+} + n_{N_2^+}$ follows from quasi neutrality. These equations are solved numerically.

Allowing some variations in the rate constants, a fit to the measured data is shown as the solid line in Fig. 3. The rates used to obtain a good fit are: $k_1 = 2\times10^{-16}$ m^3s^{-1}, $k_2 = 1\times10^{-16}$ m^3s^{-1} and $k_3 = 0.5\times10^{-13}$ m^3s. These values compare reasonably to the theoretical values given above. The same rate constants are used to calculate the ion to electron mass ratio in the plasma. This is shown in Fig. 5(b). According to theory [1] the mass ratio determines the ratio of electron to ion saturation currents in single Langmuir probe measurements. These experimentally determined ratios are shown in Fig. 5(a). Although the measured and the calculated ratios differ in absolute value, the trend towards lighter ions is visible. The difference in absolute values is possibly caused by small offsets in the measuring circuitry, which has great influence on the ion saturation current and therefore on the current ratio.

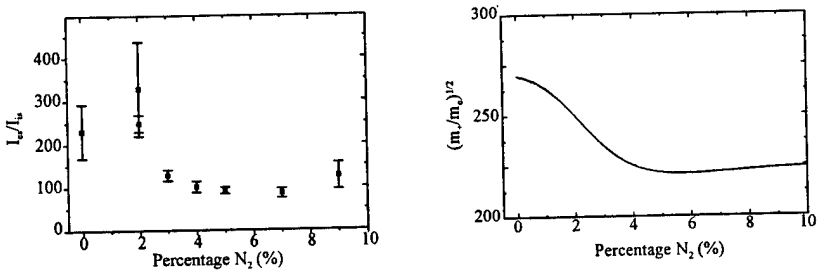

Figure 5: Electron to ion saturation current (a) and calculated mass ration (b) as a function of relative nitrogen flow.

The model predicts that at seeding percentages of nitrogen larger than approximately 10% the plasma will consist of predominantly N_2^+ ions. The plasma density downstream drops to below 10^{17} m^{-3}. At these low electron densities the dissociative recombination becomes small. The plasma density as a function of distance from the nozzle with a nitrogen seeding of 80% is shown in Figure 6, where the solid line is an apparent linear fit resulting in a 1/*e* decay length of 9 cm. This decay length is comparable to the one found in argon [10 cm, see Figure (2)], since the N_2^+ ions will have resonant charge exchange with the N_2 in the background, similar to Ar^+ in argon. The diffusion coefficient of N_2^+ is expected to be higher by a factor of 40/28 (the mass ratio), but this will be partly compensated by a higher drift velocity.

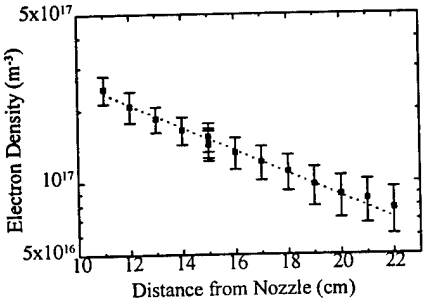

Figure 6: Electron density as a function of distance from the nozzle in a 80% nitrogen-argon plasma. The dashed line shows exponential decay with an effective decay length of 9 cm.

The results obtained here with the plasma in the low flow regime can be compared to results found by Dahiya et al. [9] in a similar plasma at much higher flow (>1000 scc/min). Although the same (charge exchange and dissociative recombination) reactions are taking place, the dominant ion found in the mass spectrometer by Dahiya et al. is N^+. This is due to the fact that the ion densities at higher flow rates are higher, typically of the order of 10^{18} m^{-3} at a distance of 20 cm from the nozzle.

V. CONCLUSIONS

It was shown that the modifications to the arc will improve the efficiency by a factor of two in the low flow argon plasma. In the case that nitrogen is seeded into the arc plasma the plasma density is lowered considerably due to charge exchange and dissociative recombination. At nitrogen flows larger than 10% the plasma density at 15 cm from the nozzle is slightly less than 10^{17} m^{-3} and does not decrease further with higher partial nitrogen flow. The dominant ion in this case is molecular ion N_2^+. Because of the low electron density at high percentages of nitrogen, the dissociative recombination becomes slow. The main loss process of ions in this case is diffusion away from the plasma axis. The effective decay length found is 9 cm comparable to the loss of Ar^+ in Ar.

ACKNOWLEDGMENTS

The authors wish to thank Gareth Ferrier and Ton Kiers for their help. The authors also thank M.J.F. van de Sande, A.B.M. Hüsken and H.M.M. de Jong for their technical assistance. This work was supported by the Netherlands Technology Foundation (STW) and the Royal Netherlands Academy of Arts and Sciences (KNAW). This work is part of a collaborative effort between Wright Patterson AFB and Eindhoven University of Technology and has been supported under the European Office of Aerospace Research and Development (EOARD) contract number SPC-95-4039.

REFERENCES

1 see for example M.A. Lieberman and A.J. Lichtenberg, Principles of Plasma discharges and material processing (John Wiley & Sons, Inc. New York, 1994).

2 M.C.M. van de Sanden, J.M. de Regt and D.C. Schram, Plasma Sources Sci. Technol. **3**, 501 (1994).

3 G.J. Meeusen, R.P. Dahiya, M.C.M. van de Sanden, G. Dinescu, Zhou Qing, R.F.G. Meulenbroeks, and D.C. Schram, Plasma Sources Sci. Technol. **3**, 521 (1994).

4. M.C.M. van de Sanden, J.M. de Regt, and D.C. Schram, Phys. Rev. E **47**, 2792 (1993).

5 M.C.M. van de Sanden, R. van den Bercken, and D.C. Schram, Plasma Sources Sci. Technol. **3**, 511 (1994).

6. W. Lindinger, F. Howorka, P. Lukac, S. Kuhn, H. Villinger, E. Alge, and H. Ramler, Phys. Rev. A **23**, 2319 (1981).

7 S.C. Brown, Basic Data of Plasma Physics, 1966, 2nd ed. M.I.T. Press, Cambridge, Massachusetts (1966).

8 J.B. Hasted, Physics of Atomic Collisions, 2nd ed. Butterworths, London (1972).

9 R.P. Dahiya, M.J. de Graaf, R.J. Severens, H. Swelsen, M.C.M. van de Sanden, and D.C. Schram, Phys. Plasmas **1**, 2086 (1994).

LASER INDUCED FLUORESCENCE MONITORING OF ATOMIC H AND N IN EXPANDING PLASMAS PRODUCED BY A CASCADED ARC

M.G.H. Boogaarts, G.J. Brinkman, S. Mazouffre, H.F. Döbele[a)], J.A.M. van der Mullen, and D.C. Schram

(Department of Applied Physics, Eindhoven University of Technology, P.O. Box 513, 5600 MB Eindhoven, The Netherlands)
a) (Institut für Laser- und Plasmaphysik Universität GH Essen, 45117 Essen, Fed.Rep.Germany)

ABSTRACT: In this contribution we present Two-photon Absorption Laser Induced Fluorescence (TALIF) measurements on expanding plasmas produced by a cascaded arc in Ar/H_2 and Ar/N_2 mixtures. From these measurements axial and radial profiles for the density, the temperature, and the radial velocity of the atomic species are obtained. Absolute number densities of atomic hydrogen are obtained, by calibrating the TALIF-signal via a titration reaction in a flow tube reactor.

I. INTRODUCTION

When a cascaded arc created plasma expands into a vacuum vessel, a versatile high quality particle beam is obtained that has been shown to have very promising features [1,2]. An important application of such an expanding plasma is its use for fast deposition of e.g. amorphous silicon (a-Si:H) or carbon (a-C:H) [2,3]. For these applications, but also from a fundamental point of view, it is interesting to study the composition of the beam, i.e. the degree of dissociation, excitation, and ionization, as a function of externally controlled parameters, such as flow, pressure, arc current, etc.

Several laser-based diagnostic techniques, like Thomson/Rayleigh scattering, CARS, and LIF are used to probe the local particle densities in the expanding plasma and their energy distribution. These techniques have the general advantage to be non-intrusive and very sensitive. However, species-selective monitoring of atoms in their ground-state requires the use of high energetic photons because of the large energy spacings involved. Experimentally demanding techniques that are necessary for single-photon excitation can be avoided with the application of multi-photon excitation.

In this contribution we present measurements on atomic H and N using two-photon excitation and detection of the resulting non-resonant laser-induced fluorescence (LIF). The corresponding energy level schemes are shown in Fig. 1. Atomic H is excited with two 205.14 nm photons from the 1s ^2S ground state to the 3d ^2D and 3s ^2S states. The excitation is monitored by detection of the fluorescence on the Balmer-a line at 656.3 nm. Atomic N is excited from the 2p $^4S^0$ ground state to

the 3p $^4S^0$ state with two 206.7 nm photons. The resulting fluorescence to the 3s ^4P states is detected around 745 nm.

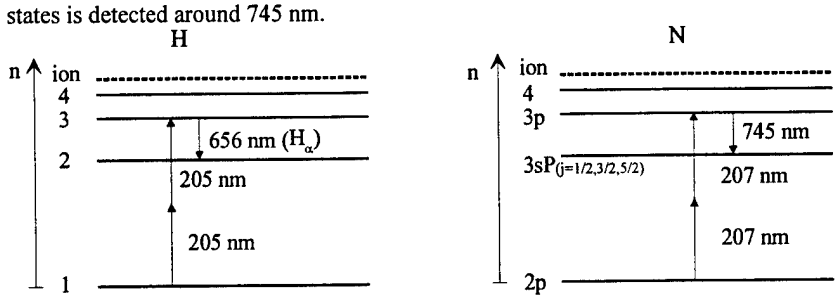

Fig. 1: Energy level schemes for the two-photon absorption laser induced fluorescence (TALIF) measurements on H (left) and N (right).

II. EXPERIMENTAL

A scheme of the experimental set-up is depicted in Fig. 2. The cascaded arc plasma source has already been described in detail elsewhere [4]. In the experiments described in this paper it is operated on a 40 A dc current. The plasma expands from a 4 mm diameter channel into a roots-blower pumped vessel with a background pressure of 10 Pa. For the measurements on H an Ar/H_2 mixture is used with 3.0 slm Ar-flow and 0.5 slm H_2-flow. The plasma conditions for this case are close to those used for deposition of a-C:H and a-Si:H. For the measurements on N a nearly 100% N_2-flow (2.0 slm) is used with only a small fraction of Ar (0.05 slm) to stabilize the plasma. The cascaded arc plasma source is mounted on a translation arm. Spatial scans through the expanding plasma can be made by moving the cascaded arc relative to the laser beam and detection optics.

The laser system that is used to produce the tunable UV-radiation is based on a pulsed Nd:YAG/dye-laser combination. The frequency-doubled output (250 mJ pulse energy) of a 50 Hz injection-seeded Nd:YAG-laser (Spectra-Physics, GCR-230) is used to pump a tunable dye-laser (Spectra-Physics, PDL-3). The dye-laser has a bandwidth of 0.07 cm^{-1} and is used around 615 nm for the measurements on H and around 618 nm for the N measurements. The output of the dye-laser (typically 60 mJ) is frequency-tripled in two stages using non-linear optical techiques. In the first stage the light is frequency-doubled in a KD*P-crystal. In the second stage this frequency-doubled UV light is mixed with the residual red dye-laser output in a BBO-crystal where typically 0.5 mJ of tunable UV light around 205 nm with an estimated bandwidth of 0.2 cm^{-1} is produced via sum-frequency generation.

The frequency-tripled laser light is imaged via a lens-pinhole-lens combination onto a 60 cm lens that focusses the light into the plasma. The laser-induced fluorescence originating from the focus is imaged with a spatial resolution of 2 mm, in a direction perpendicularly to the laser beam, onto a photo-multiplier (Hamamatsu, R928). The continuous background light emitted by the plasma is strongly reduced by

an optical filter in front of the photo-multiplier tube (PMT). In case of the H-fluorescence a H_a bandpass filter is used, whereas in the case of N-fluorescence a highpass filter is used that is transparant above 730 nm. The background signal is further reduced by accumulating the PMT-signal with a gated integrator only during a preset time interval of some 200 ns after the arrival of the laser pulse. The resulting signal is digitized by a CAMAC converter, and then read into a PC that also controls the wavelength scanning of the dye-laser.

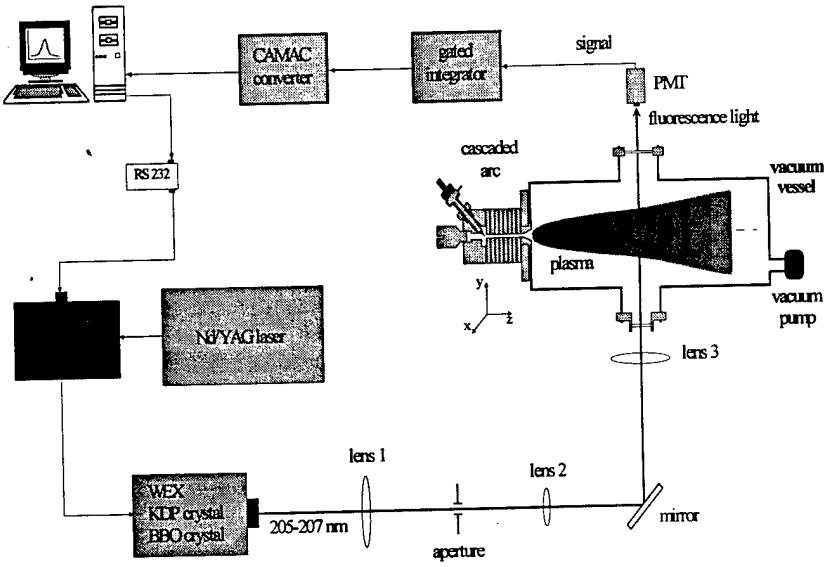

Fig. 2: Scheme of the experimental set-up. The cascaded arc plasma source is mounted on a translation arm that allows for spatially resolved measurements.

III. CALIBRATION

All fluorescence measurements are obtained by tuning the excitation laser and recording the resulting spectral profile of the two-photon absorption for various axial and radial positions. The spectral scans are all fitted to a Gaussian profile. From these fits three local parameters can be obtained in principle. The local density is obtained from the integrated intensity (i.e. the area under the curve), while the local temperature is derived from the Doppler-width of the spectral profile. In addition, the component of the velocity in the direction of the laser can be determined from the absolute shift of the center frequency of the spectral profile.

In order to obtain quantitative velocity data, the wavelength of the laser needs to be calibrated. In our experimental set-up such a calibration will yield the values for the radial velocity of atomic H and N. A calibration based on the simultaneous

measurement of the absorption spectrum of I_2 is currently being implemented. In addition, we plan to measure the axial velocities by applying the excitation laser anti-parallel or under a small angle with the symmetry axis of the expansion.

The density profiles measured via TALIF are relative. To obtain absolute atomic number densities, the TALIF-setup needs to be calibrated against an independent source that produces a well-known amount of the atomic species. For H this has been done via a titration in a flow tube reactor [5]. Atomic H is produced in the flow tube reactor in a diluted He/H_2-flow by dissociation of the molecular H_2 in a microwave cavity. The atomic H is then transported by the He-flow via an inert tube to a position close to the scattering volume of the laser. To determine the amount of H produced, the fast titration reaction $H + NO_2 \rightarrow NO + OH$, with a rate of $1.3.10^{-10}$ cm^3/s.molecule, has been used [5]. By scaling the resulting H-density with the ratio between the integrated TALIF intensity of the cascaded arc plasma and that of the flow tube reactor, we are able to determine the spatially-resolved absolute H number density in the expanding Ar/H_2 plasma. The accuracy of the density values is about 50%, which is mainly due to the incertainty in the determination of the pressure in the vessel. Calibration of the N-density in the Ar/N_2 plasma, although less straightforward, will be conducted in a similar way.

The absolute number densities of the atomic species are not only important to gain information on the fundamental plasma processes and conditions, like the degree of dissociation, but also to obtain a quantitative idee of the sensitivity of the TALIF technique for the various atomic species.

IV. RESULTS

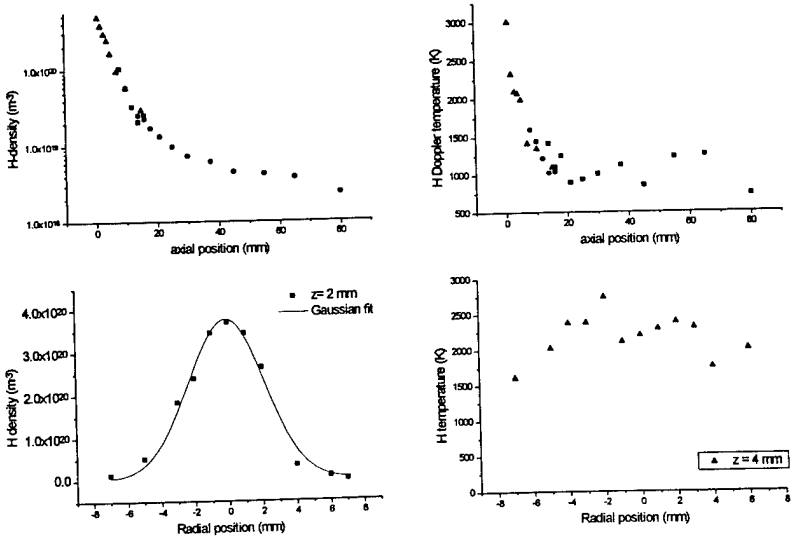

Fig. 3: Axial (upper) and radial (lower) profiles of the density (left) and temperature (right) of atomic H. The radial scans are taken at a axial distance from the nozzle of z=2 mm (left) and z=4 mm (right).

The axial and radial profiles of the density and temperature of atomic H are shown in Fig. 3. The H-density on the axis is about 5.10^{20} m^{-3} close to the nozzle, and decays rapidly with distance from the nozzle. In the first part of the expansion the axial density profile can be fitted well to an exponential decay with a 1/e length of 4 mm. For distances above 30 mm, the H density starts an asymptotic behaviour. To determine the 'residual' H-density that probably will be constant throughout the vessel, the measurements need to be extended to still larger distances. The temperature on the axis starts at about 3000 K near the nozzle and decreases until a minimum of about 1000 K is reached at a distance of 20 mm. Then the temperature slightly increases again and finally levels of at about 1100 K.

Radial scans are measured up to 8 mm from the nozzle. They show for the density a Gaussian-like shape with a clear maximum in the centre and for the temperature a plateau in the centre with the temperature falling down at the edges. The axial line density, that is the density integrated over one radial plane, appears to be almost constant. Assuming that the axial velocity is constant, this implies that the total amount of atomic hydrogen is conserved during the expansion.

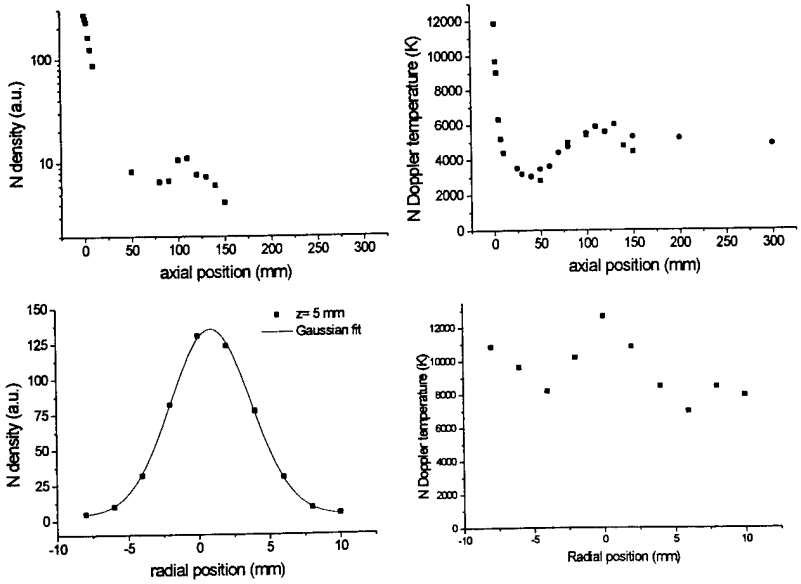

Fig. 4: Axial (upper) and radial (lower) profiles of the density (left) and temperature (right) of atomic N. The radial scans are taken at z =5 mm.

For atomic N the axial and radial profiles of the density and temperature are shown in Fig. 4. Both the axial density and temperature profile show evidence of a shock region at about 100 mm from the nozzle. The radial density profiles are again well approximated by a Gaussian, while the radial temperature profile is less well-behaved.

V. CONCLUSIONS

Two-photon excitation laser induced fluorescence measurements enable the spatially-resolved determination of the density, the temperature, and the velocity of atoms in e.g. expanding plasma's. The TALIF technique has been applied to monitor atomic hydrogen and nitrogen in the expanding plasma of a cascaded arc burning on Ar/H_2 and nearly pure N_2, respectively.

The setup has been calibrated for H using a titration in a flow tube reactor. The H number density in the Ar/H_2 plasma has a maximum of 5.10^{20} m^{-3} near the nozzle for operating conditions that are typical for deposition research.

From these measurements it is concluded that the detection limit of our TALIF setup for atomic hydrogen lies well below a density of 5.10^{17} m^{-3}.

The interpretation of the data in terms of dissociation efficiency and net atomic flux of the cascaded arc is currently being undertaken. For this it is also important to measure the axial velocities of the atoms, which is one of the next objectives of our research.

ACKNOWLEDGEMENT

This work is financially supported by the "Stichting Technische Wetenschappen (STW)". The authors would like to thank Dr. U. Czarnetzki and coworkers at the University of Essen for using their flow tube reactor, and H.M.M. de Jong, M.J.F. van de Sande and A.B.M. Hüsken for their skillful technical assistance.

REFERENCES

[1] Meulenbroeks RFG, Engeln RAH, Beurskens MNA, Paffen RMJ, van de Sanden MCM, van der Mullen JAM, Schram DC. Plasma Sources Sci. Technol., 1995, 4: **74**

[2] van de Sanden MCM, Severens RJ, Meulenbroeks RFG, de Graaf MJ, Qing Z, Otorbaev DK, Engeln R, Gielen JWAM, van der Mullen JAM, Schram DC. Suface and Coatings Technology, 1995, 74-75: **1**

[3] van de Sanden MCM, Severens RJ, Gielen JWAM, Paffen RMJ, Schram DC. Plasma Sources Sci. Technol., 1996, 5: **268**

[4] van de Sanden MCM, de Regt JM, Janssen GM, van der Mullen JAM, Schram DC, van der Sijde B. Rev. Sci. Instum., 1992, 63: **3369**

[5] Setser DW. Reactive Intermediates in the Gas Phase. New York: Academic Press, 1979

HIGH RATE DEPOSITION OF AMORPHOUS HYDROGENATED SILICON USING AN EXPANDING THERMAL PLASMA

R.J. Severens, W.M.M. Kessels, L. Gabella, F. van de Pas,
M.C.M. van de Sanden, D.C. Schram
(Department of Applied Physics, Eindhoven University of Technology,
P.O. Box 513, 5600 MB Eindhoven, The Netherlands)

ABSTRACT: Using an expanding cascaded arc plasma we have achieved to grow device quality a-Si:H at a deposition rate of over 10 nm/s. A residual gas analyzer provides information concerning the plasma chemistry, whereas substrate temperature dependencies of the growth rate, refractive index and electronic properties supply input data for a growth model.

I. INTRODUCTION

Production cost reduction is the essential step in the commercialization of photovoltaic devices. Amorphous hydrogenated silicon (a-Si:H) is of special interest, since it can be deposited over large areas and allows fairly easy scale-up, but as yet, a-Si:H solar cells cannot compete with conventional means of electricity generation. Increasing the deposition rate can lead to an additional cost reduction, since the same production line througput can be obtained at lower investment cost. A requirement, however, is that the quality of the deposited material remains suitable for use in photovoltaic devices. Apart from economic significance, the study of very-high-rate deposition of a-Si:H is also of scientific interest, since growth models can be tested under more extreme conditions.

As a basis, we use the model reported by Matsuda and Ganguly [1] -also proposed by Perrin [2] and Gallagher [3] as it succeeds to explain most observed phenomena [4]. The principle of the MPG-model is schematically represented in Fig. 1. Physisorbed SiH_3 radicals are assumed to be the only particles involved in the growth process. They hop across the practically fully hydrogenated surface until they either find a dangling bond and stick, generate a dangling bond by abstraction of a surface hydrogen atom, or recombine with another SiH_3 radical to form Si_2H_6. At elevated temperatures, also thermal desorption of surface hydrogen becomes a source for surface

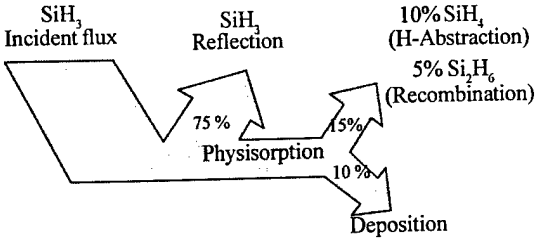

Fig. 1. Schematic representation of the MPG model

dangling bonds: Matsuda reports an increase of the growth rate from 0.04 at 350 ^{0}C to 0.13 nm/s at 450 ^{0}C [1]. The model predicts a factor 2.5: at a high temperature, also the abstraction/recombination radicals will stick and contribute to growth. The enhanced dangling bond generation also causes the photo conductivity to decrease. If however the incident SiH_3 flux is increased, faster 'passivation' reduces the dangling bond generation due to thermal desorption: the model -correctly- predicts a recovery of the photo conductivity.

So far the model has been succesfully used to explain data originating from a 13.56 Mhz triode PECVD-reactor, with growth rates in the range 0.02-1.5 nm/s. In this contribution, growth data will be presented for a-Si:H films deposited using an expanding thermal plasma, in the range 0.3-50 nm/s.

II. EXPERIMENTAL SETUP

The plasma source of this remote plasma deposition setup consists of a DC thermal arc operated at 0.5 bar and 5 kW [5], which is fed with an argon/hydrogen (or, for isotope labeling, argon/deuterium) with a total flow of around 4 SLM. Differential pumping maintains the pressure in the deposition chamber at about 0.2 mbar (Fig. 2), thus creating a plasma jet with a typical flow velocity of 10^3 m/s. Typically 0.6 SLM of pure silane (or SiD_4) is injected through a ring at 45 mm from the nozzle of the source. The substrates, Corning 7059 glass and c-Si mounted onto a substrate holder, are inserted into the deposition chamber through a load lock system and actively clamped onto a copper yoke at a distance of 32 cm from the source. The yoke is temperature controled and features helium backflow for enhanced thermal contact between yoke, holder and substrates.

Attached to the deposition chamber is a Balzers QMS 200 Prisma residual gas analyzer (RGA), with which the consumption of silane and the production of hydrogen

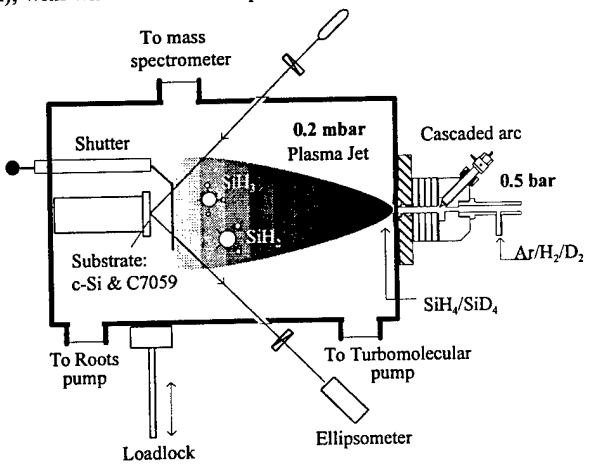

Fig. 2. Expanding Thermal Plasma deposition setup

due to ignition of the plasma are monitored. Film growth rate and refractive index at 632.8 nm are determined in-situ using a Rotating Compensator Ellipsometer. Ex-situ Fourier Transform Infra Red transmission (FTIR) measurements yield the infrared refractive index and the SiH, SiH_2, SiD, SiD_2 and SiHD bond concentrations. The total hydrogen and deuterium content and the silicon density are determined using combined Elastic Recoil Detection Analysis (ERDA) and Rutherford Backscattering Spectrometry (RBS) with 4MeV He^+-ions. The photo conductivity is obtained under global AM1.5 illumination using coplanar aluminum contacts; the dark conductivity and its activation energy are determined from a conductivity vs. temperature scan. The Tauc optical bandgap is calculated from reflection/transmission spectra.

III. SILANE CONSUMPTION

Deposition of a-Si:H on the substrates and the vessel walls leads to a decrease of the silane partial pressure, which can be monitored using the RGA. The (absolute) partial pressure change is a direct measure for the growth rate, expressed in atoms/sec. The silane consumption is defined as the (relative) fraction of the silane flow that is deposited. Fig. 2 shows the silane consumption as a function of hydrogen flow for three arc currents (30, 45 and 75 A); the silane flow was constant at 10 scc/s. Two regions can be distinguished, indicated by A and B: in region A, the ion flux coming out of the arc is high and so is the silane consumption. The dominant reactions are charge exchange and dissociative recombination [5]. Note that electrons do not contribute to silane consumption: the electron temperature is low (<0.5 eV) and the flux of tail electrons is negligible. In region B, the ion flux is quenched by addition of hydrogen: now the hydrogen atom becomes the dominant chemically active species, and silane is dissociated by the abstraction reaction

$$SiH_4 + H \rightarrow SiH_3 + H_2 \quad (\Delta H = -0.5eV) \tag{1}$$

Since the H-flux increases with H_2-flow, region B shows an increase of the silane consumption. Obviously, with increasing arc current, the ion flux coming out of the arc increases and so does the silane consumption; at 75 A, the quenching is not complete even at $H_2 = 10$, and both ions and H-atoms play a role.

Note that every consumed silane molecule effectively generates one H_2 molecule -this has been verified with the RGA- since deposition on the cold vessel walls leads to polymer-like a-Si:H with SiH_2 stoichiometry. This means that even without H_2 addition to the arc, up to 10 scc/s H_2 is generated in the deposition chamber itself! From Fig. 3 it can however be concluded that *this* H_2 does not have the same quenching effect as H_2 fed to the arc, otherwise the silane consumption without H_2 fed to the arc could not be so much higher than at H_2=5 scc/s.

In some cases, the silane depletion approaches 100%. In that case, the mass spectrometer signal ratio of mass 31 (SiH_3^+) over mass 30 (SiH_2^+), which is according to the fragmentation pattern of SiH_4 in the ionizer 0.8, starts decreasing (Fig. 4). This could indicate that the sampling gas is no longer dominated by SiH_4 but by a lower

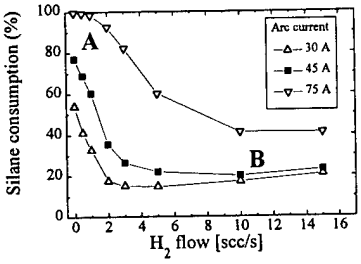

Fig. 3. Consumption of silane vs. hydrogen flow for arc currents of 30, 45 and 75 A. The silane flow is fixed at 10 scc/s.

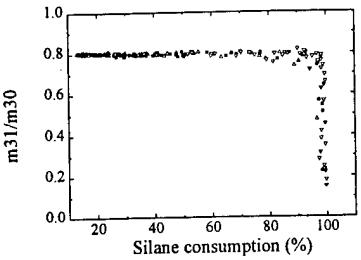

Fig. 4. Mass spectrometer signal ratio of mass 31 over mass 30 vs. silane consumption. Both hydrogen and silane flows have been varied; arc currents are 30, 45 and 75 A

silane such as SiH_2. In the next section we will see that in a condition with such a high depletion, very poor quality material is deposited.

IV. GROWTH OF a-Si:H

Fig. 5 shows the temperature dependence of the growth rate for a number of plasma settings as indicated in Table 1. The SiH4:H2 setting is referred to as 'standard'. In one series, the hydrogen has been replaced by deuterium and, since the plasma source operates more efficiently on deuterium, the silane consumption and thus the growth rate increases. Furthermore a series with extremely high growth rate, a low growth rate and very low growth rate are presented. In the 'ultralow' and even in the low rate series, we observe a slight increase of the growth rate at elevated temperatures, according to the model, due to increased dangling bond generation as a result of thermal desorption of hydrogen. Such an increase cannot be seen in the other series, where the radical flux is higher. Indeed we also observe the corresponding optimum in the photo conductivity (Fig. 7), which shifts to a higher substrate temperature when the radical flux is increased - some film properties of the sample deposited under standard conditions and at Tsub=475 ^{0}C are given in Table 2. The photo conductivity behavior clearly shows that if the growth flux is low, the dangling bond density does increase at high temperatures. However, in the ultralow rate series, the growth rate does not increase by the expected factor of 2.5, but only by 10%. This suggests that in our setup, only few radicals are responsible for dangling bond generation by surface hydrogen abstraction, and most of the physisorbed radicals stick. An alternative dangling bond generation mechanism could be abstraction by free atomic hydrogen in the plasma,

Table 1. Deposition settings for the presented series.

	I_{arc} (A)	H_2 (scc/s)	SiH_4 (scc/s)
SiH_4:H_2	45	10	10
SiH_4:D_2	45	10 (D_2)	10
highrate	25	0	15
lowrate	25	5	3
ultralow	10	3	0.6

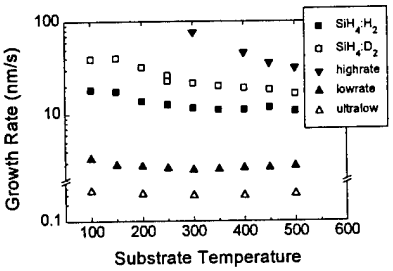

Fig. 5. Substrate temperature dependence of the growth rate

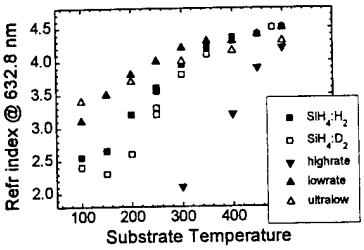

Fig. 6. Substrate temperature dependence of the refractive index at 632.8 nm

possibly through a physisorbed state. That the surface is exposed to such atoms is proven by the deuterium experiment, where we found that 10% of the incorporated hydrogen is in fact deuterium - this also shows that practically all hydrogen in a-Si:H comes from silane. In the cross-reference experiment where we used SiD_4 and H_2, we found 10% hydrogen in deuterium.

Such a mechanism of physisorbed hydrogen could also explain why at low temperatures, the growth rate decreases with increasing temperature. Even though most of the effect can be attributed to the material becoming more dense -Fig. 6 clearly shows the increase of the refractive index with temperature-, ERDA and RBS still indicate that the effective growth flux becomes lower as the temperature goes up. What could happen is that the physisorbed hydrogen and the physisorbed SiH_3 radical recombine to form desorbing SiH_4 without generating a dangling bond. Since the surface diffusion velocity increases with temperature, one could expect a consequent decrease of the growth rate. In the deuterium experiment, the described mechanism would lead to the production of SiH_3D, and indeed its presence has been demonstrated with the RGA.

Fig. 6 also shows that the slope of the refractive index increase with temperature, depends on the growth rate. Again this may be due to the need for surface migration in order to get proper, conformal growth. Still, temperature and growth rate are not the only determining parameters, as is indicated in Fig. 8. Here, the temperature was kept constant at 310 ^{0}C, and the arc current remained 45A. By varying the hydrogen and silane flows, the growth flux could be modified. The highest refractive index corresponds to the conditions with low relative silane consumption. The low rate conditions at the left side all have a higher silane consumption fraction -the arrow indicates a condition with 100% silane depletion- and show a lower refractive index. From this we tentatively conclude that a high silane consumption may be indicative of the formation of lower silane radicals, which, by their lower surface mobility, produce low quality material.

Table 2. Film properties using standard condition at T_{sub}=475 ^{0}C

growth rate	11 nm/s	$E_{gap,\ Tauc}$	1.63 eV
n_{HeNe}	4.4	σ_{photo}	$6\times10^{-5}\ \Omega^{-1}cm^{-1}$
n_{IR}	3.7	$\sigma_{photo}/\sigma_{dark}$	2×10^{4}
[H]	6%	E_{act}	0.74 eV
$I_{2100}/(I_{2000}+I_{2100})$	0.1		

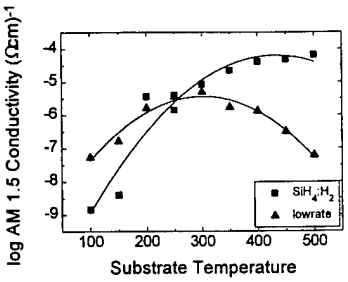

Fig. 7. Logarithm of the photo conductivity vs. substrate temperature for the low rate series and the standard series. As the growth rate increases, the optimum shifts to a higher temperature.

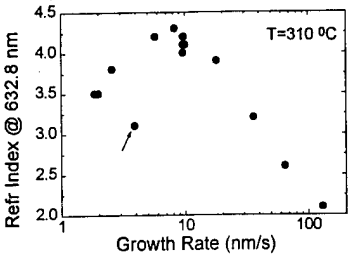

Fig. 8. Refractive index vs. growth rate at T_{sub}=310 ^{0}C, by varying the hydrogen and silane flow at constant arc current. The arrow indicates a condition with 100% silane consumption.

ACKNOWLEDGEMENT

This research is financially supported by the Netherlands Agency for Energy and the Environment (NOVEM), the Netherlands Organization for Research (NWO), the Foundation for Fundamental Research of Matter (FOM-RG) and the Royal Netherlands Academy of Arts and Sciences (KNAW). The authors wish to thank M.J.F. van de Sande, A.B.M. Hüsken and H. de Jong for their skillful technical assistance.

REFERENCES

[1] Matsuda A, Nomoto K, Takeuchi Y, Suzuki A, Yuuki A, Perrin J. Surface Science 227, 50-56 (1990); Ganguly G, Matsuda A. J. Non-Cryst. Solids 164-166, 31-36 (1993); Jpn. J. Appl. Phys. **31**, L1269-L1271 (1992); Mat. Res. Soc. Symp. Proc. 258, (1992)

[2] Gallagher A. Mat. Res. Soc. Symp. Proc. 70, 3-10 (1986)

[3] Perrin J, Takeda Y, Hirano N, Takeuchi Y, Matsuda A. Surface Science 210, 114-128 (1989); Perrin J. Reactor Design for a-Si:H Deposition, in Plasma Deposition of Silicon-Based Materials. New York: Academic Press (1995)

[4] Severens RJ, Van de Sanden MCM, Verhoeven HJM, Bastiaanssen J, Schram DC. Mat. Res. Soc. Symp. Proc. 420, 341-346 (1996)

[5] Severens RJ, Brussaard GJH, Verhoeven HJM, Van de Sanden MCM, Schram DC. Mat. Res. Soc. Symp. Proc. 377, 33-38 (1995)